Average magnetotail electron and proton pitch angle distributions from Cluster PEACE and CIS observations

A. P. Walsh,[1] C. J. Owen,[1] A. N. Fazakerley,[1] C. Forsyth,[1] and I. Dandouras[2]

[1] We present results from the first systematic survey of proton and electron pitch angle distributions in the magnetotail, based on Cluster CIS and PEACE data binned by proton plasma β (β_p). The proton distributions conform to the canonical picture of magnetotail ions - a boundary layer made up of Earthward streaming and bidirectional field-aligned particles, consistent with recent observations of time-varying beamlets, which gives way to a broadly isotropic central plasma sheet when $\beta_p \sim 3$. The electron distributions are significantly different from the canonical picture. A "boundary layer" made up of bidirectional field-aligned electrons is observed to values of β_p as high as 17. This boundary quickly gives way to perpendicular-dominated electrons close to the neutral sheet. Hence, our results suggest that, on average, there is no extended, isotropic electron plasma sheet and that the proton plasma sheet is not routinely encountered until higher β_p than commonly assumed. **Citation:** Walsh, A. P., C. J. Owen, A. N. Fazakerley, C. Forsyth, and I. Dandouras (2011), Average magnetotail electron and proton pitch angle distributions from Cluster PEACE and CIS observations, *Geophys. Res. Lett.*, *38*, L06103, doi:10.1029/2011GL046770.

1. Introduction

[2] In the canonical view of the magnetosphere, the magnetotail is divided into four regions: the north and south lobes, the plasma sheet boundary layer (PSBL) and the central plasma sheet (CPS). The lobes, comparatively empty of plasma, are on open magnetic field lines. The PSBL lies on newly-closed field lines and is generally characterized by uni- or bidirectional beams of field-aligned particles. More recently, the ion beams observed in the PSBL have been explained as "beamlets", time-varying velocity dispersed structures that originate from many different points in the CPS [e.g., *Ashour-Abdalla et al.*, 2005], suggesting the PSBL is a dynamic interface between the lobes and CPS, rather than a distinct static layer. The CPS itself, existing closest to the center of the magnetotail, is usually characterized by more isotropic ion and electron distributions [e.g., *Parks et al.*, 1984].

[3] The physical processes that act to isotropize PSBL particle distributions such that they might contribute to the CPS distributions are still not fully understood or conclusively identified. Candidates include the acceleration of particles as they pass through the distant or near-Earth neutral lines and associated velocity-filter and time-of-flight effects [e.g., *Onsager et al.*, 1991]; nonadiabatic acceleration in current sheets [*Tsyganenko*, 1982] and wave-particle interactions [e.g., *Parks et al.*, 2001].

[4] Since the initial characterization of the magnetotail, which was based on the results of case studies, much work has been devoted to studying its bulk properties. *Baumjohann et al.* [1988, 1989], defined an outer CPS where $0.5 < \beta < 3.0$ and an inner CPS where $\beta > 3.0$, where β is the ratio of plasma and magnetic pressures. This led to the commonly used criterion that the ion $\beta > 0.5$ in the CPS [e.g., *Angelopoulos et al.*, 1992]. The distribution functions of ions [e.g., *Parks et al.*, 2001] and electrons [*Smets et al.*, 1999] under specific circumstances has also been studied. However, little work has been done to investigate the average particle pitch angle distributions (PADs) in the magnetotail in a statistical way. In this letter we report results from the first systematic survey of magnetotail PADs measured by Cluster between 15 and 19 R_E from the Earth.

2. Data Selection and Processing

[5] Here we survey 2D PADs of protons measured by the CIS-CODIF instrument [*Rème et al.*, 2001] and electrons measured by the PEACE instrument [*Johnstone et al.*, 1997] taken from the Cluster 4 (C4) spacecraft during the 2002 tail season. PEACE returns a PAD every spin (~4 s) and CODIF usually returns a PAD every two spins. PADs will be discussed in terms of differential energy flux (dEF, keV cm^{-2} s^{-1} sr^{-1} keV^{-1}) throughout this letter and have been analyzed in the spacecraft frame. We bin each distribution by the concurrent proton β (β_p). β_p was chosen because it is a popular identifier of the CPS and in this study we are able to check its validity in distinguishing between magnetotail regions. We note that β_p is not independent of proton dEF, but it also involves magnetic field and is a scalar quantity. We primarily examine the PADs in terms of the difference between their field-aligned and perpendicular components, so β_p is a suitable binning quantity.

[6] In order to ensure the surveyed PADS were representative of the CPS and PSBL, we restricted our survey to those times when C4 was located at $R > 15 R_E$ in the tail on days 200–300. Plasma sheet intervals (±~1 hour) were selected by inspection of summary plots. These were then restricted to times at which CODIF measured $0.01 < n_p < 10$. This ensures sufficient counting statistics such that we can be confident in the calculated values of β_p, while disregarding anomalous data spikes. Those orbits with data gaps that would complicate data processing were disregarded. In total data from 33 orbits were included, encompassing ~700,000 electron PADs and ~350,000 proton

[1]Mullard Space Science Laboratory, University College London, Dorking, UK.
[2]Centre d'Etude Spatiale des Rayonnements, UMR 5187, Université de Toulouse, CNRS, Toulouse, France.
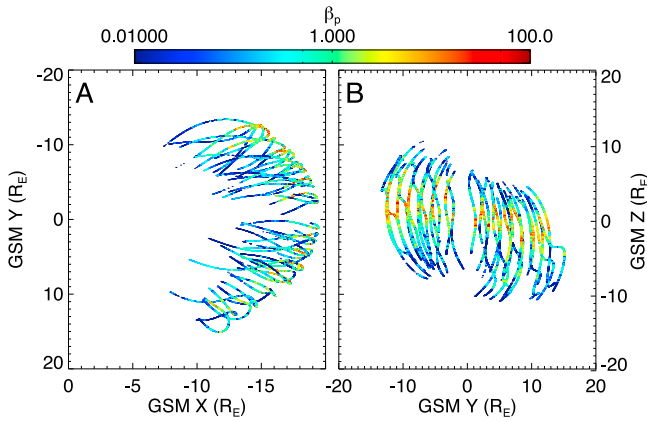
Figure 1. C4 orbit during the survey period plotted in GSM coordinates. The color scale represents β_p.

PADs. For electron PADs, those energy bins below the instantaneous spacecraft potential (SCP), as measured by EFW [*Gustafsson et al.*, 2001] and corrected according to the results of *Cully et al.* [2007], were discarded in order to remove the majority of spacecraft photoelectron contamination. Those energy/pitch angle bins below the calculated minimum background (PEACE) or one count level (CODIF) were set to zero but still included. The spatial distribution of sampling points, color-coded by β_p, is plotted in Figure 1; Figures 1a and 1b are respectively the GSM XY and YZ projections of C4's orbit. The position of the peak β_p in the YZ plane is further north in the dawnward sector than the duskward, reproducing the current sheet geometry reported by *Zhang et al.* [2006]. The gap in coverage around the noon-midnight meridian is a result of disregarding orbits with lengthy eclipses and hence data gaps.

[7] In order to compare and examine average PADs in terms of β_p, proton PADs and moments, and magnetic field vectors measured by FGM [*Balogh et al.*, 2001] were all interpolated to the same time grid as the electron PADs. Pitch Angle 0° and 180° data were then rearranged such that an array of field-aligned Earthward fluxes and an array of field-aligned tailward fluxes were generated (henceforth referred to as Earthward and tailward, respectively). The dataset was split into 100 equally-sized β_p bins in log space, the center of the lowest bin corresponding to $\log_{10}(\beta_p) = -2$ and the highest to $\log_{10}(\beta_p) = 2$. This provides a more even distribution of samples than binning in linear space. The mean of the individual PADs in each $\log_{10}(\beta_p)$ bin was then calculated along with the ratios $\langle Earthward\rangle/\langle tailward\rangle$ and $(\langle Earthward\rangle + \langle tailward\rangle)/(2\langle perpendicular\rangle)$. This was done after averaging so that individual PADs with zero flux could be included without their dominating the averages and producing infinite ratios. Note that in all cases data are taken from individual pitch angle bins rather than integrations of PADs over the relevant angle ranges and that the perpendicular data represent one gyrophase (within the limit of instrument resolution) rather than an average of an entire particle gyration.

3. Results

[8] The resulting mean proton PADs are plotted in Figure 2. Figures 2a–2c are spectrograms of the mean dEF

in the Earthward, perpendicular and tailward directions, respectively. Figure 2d is a spectrogram of the ratio between Earthward and tailward proton flux, with a color scale such that blue indicates higher Earthward fluxes, red higher tailward fluxes and green balanced fluxes. Figure 2e is a spectrogram of the ratio between the average of the Earthward and tailward proton fluxes and the perpendicular proton flux, with a color scale such that blue indicates a (anti)parallel-dominated PAD, red a perpendicular-dominated and green an isotropic PAD. Grey regions are where the average flux is below the background (2.3×10^6 keV cm^{-2} sr^{-1} s^{-1} keV^{-1}). The black trace on Figure 2f is a histogram of the number of samples in each β_p bin and the red trace shows the number of orbits from which the data in each bin were taken.

[9] Figures 2a–2c show a generally increasing proton energy flux with increasing β_p. Also evident is an energy dispersion with β_p at the low β_p end of the distribution. The low energy cutoff for fluxes $>1 \times 10^8$ keV cm^{-2} s^{-1} sr^{-1} keV^{-1} decreases with increasing β_p for Earthward-directed protons at values of β_p between 0.1 and 1.0 (Figure 2a) while the equivalent high energy cutoff increases with increasing β_p for values of $\beta_p < 0.5$. This latter effect is present in
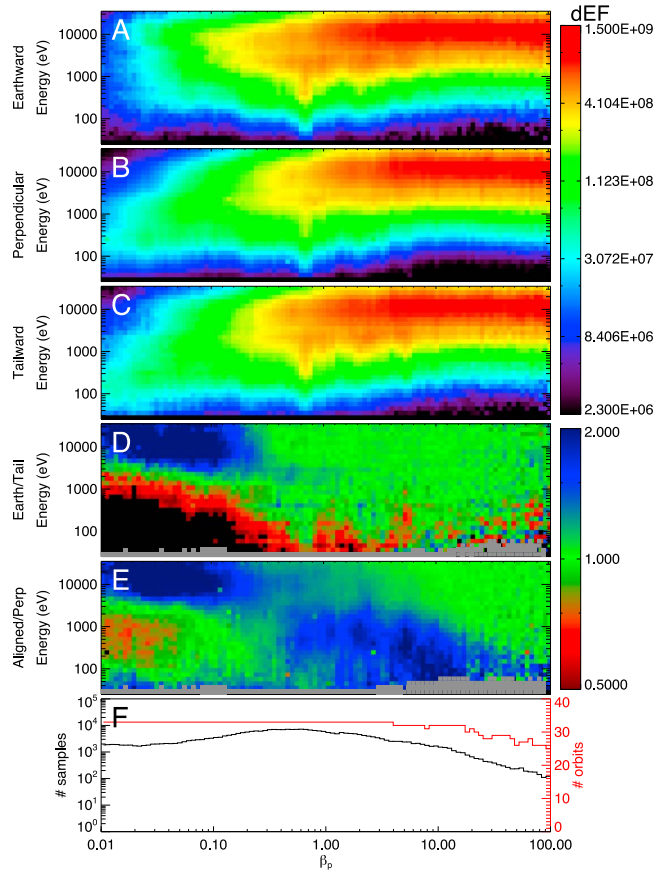
Figure 2. Proton dEF binned by β_p. (a) An Energy-β_p spectrogram of Earthward-directed field-aligned proton dEF, (b) perpendicular and (c) tailward dEF. (d) The ratio between Earthward and tailward dEF, and (e) the ratio between the mean of Earthward and tailward dEF and the perpendicular dEF. The black trace on Figure 2f is the number of samples in each β_p bin and the red the number of orbits from which the data in each bin were taken.
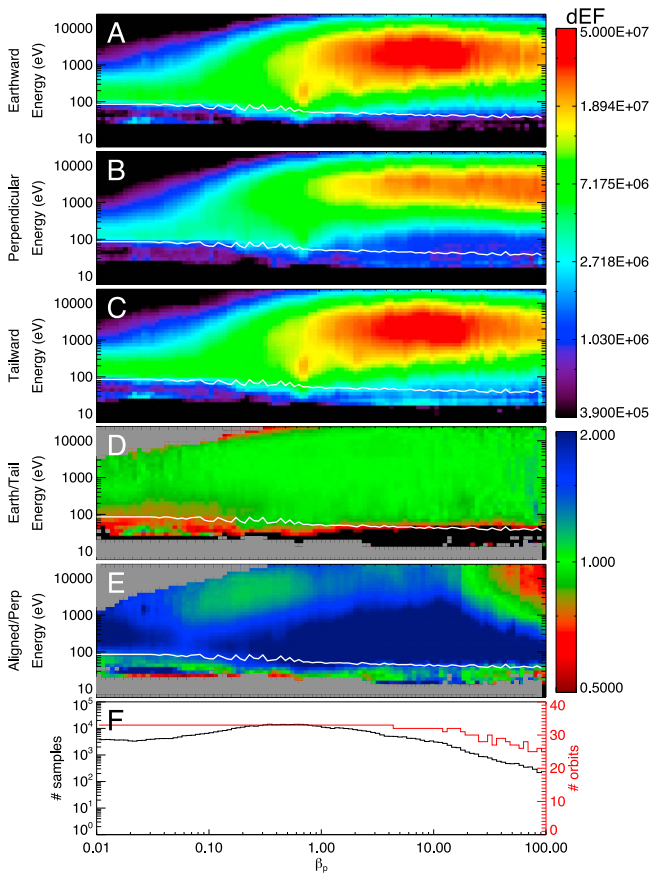
Figure 3. Electron dEF binned by β_p. Units and panels as for Figure 2. The maximum value of SCP observed in a particular β_p bin is overplotted in white on each spectrogram.

Figures 2a–2c but is stronger for PA 90° and tailward protons.

[10] At values of $\beta_p < 0.3$ there is a marked difference in the Earthward-tailward flux ratio with energy (Figure 2d). At energies >3 keV the proton dEF is heavily biased in favor of Earthward-flowing particles, whereas for protons with energy <3 keV the dEF ratio is heavily biased in favor of tailward-flowing particles. For values of $\beta_p > 0.3$, at energies above ~100 eV there is approximate balance between Earthward and tailward fluxes of protons. Note that the black area at low energy and low β_p on Figure 2d is a result of color scale saturation, implying dominance of tailward particles.

[11] At values of $\beta_p < 0.3$ there is also a marked difference in the field aligned to perpendicular flux ratio with energy (Figure 2e). At higher energies the excess Earthward flux translates to a field aligned-dominated PAD, whereas at lower energies the PAD is perpendicular-dominated. The bias in favor of field-aligned energy flux at high energies (i.e., >3 keV) extends to values of β_p up to 3, although the bias reduces with β_p. This suggests a PAD dominated by bidirectional protons at high energies for $0.3 < \beta_p < 3.0$. At lower energies the dominance of bidirectional particles continues until $\beta_p \sim 10$, although low fluxes suggest these particles do not contribute significantly to the overall dis-

tribution at energies <100 eV. At higher energies the proton PAD is isotropic where $\beta_p > 3.0$.

[12] Figure 3 is the same format as Figure 2 but shows results for electrons. The maximum SCP measured in a given β_p bin is also plotted on each spectrogram as a white trace. Ideally, electrons with energies above this line would not be spacecraft photoelectrons, however the narrow band of red just above the SCP in Figure 3d, indicating a higher tailward flux (i.e., more electrons on the Sunward side of C4) suggests that some photoelectrons have not been properly discarded and that SCP is sometimes underestimated by EFW. It is known that EFW measurements of SCP saturate at 70 eV, which can be seen in the low β_p bins on Figure 3. At high β_p, the majority of the electron dEF is measured at energies >100 eV, so this has a minimal effect on our results.

[13] As with the protons, electron fluxes increase with increasing β_p (Figures 3a–3c) and there is a similar dispersion of the maximum energy at which significant dEF is observed with β_p to that seen in the CODIF data. Additionally, both Earthward and tailward streaming electrons with a consistent peak flux energy of ~300 eV are present where $\beta_p < 0.05$.

[14] At high energies and low β_p, there appears to be a bias toward tailward streaming electrons. This is an instrument effect: sunlight in the aperture of the PEACE HEEA sensors causes contamination that is only significant for low natural fluxes of electrons. For $\beta_p > 0.3$ there is no bias in favor of either Earthward or tailward electron flux, suggesting bidirectional electrons.

[15] Unlike the protons, there is no extended region of isotropic electron PADs (Figure 3e). At low energies, field aligned electron fluxes dominate for all values of β_p and at all energies for $0.7 < \beta_p < 17$. The isotropic region at higher energies where $\beta_p < 0.7$ represents the high energy tail of the distribution. At higher energies, for $\beta_p > 17$, the electron PADs change over a narrow range of β_p to become dominated by perpendicular flux.

[16] From the red trace on Figures 2f and 3f, it can be seen that for each β_p bin data have been taken from at least 25 orbits, while for values of $\beta_p < 5$ data were taken on all 33 orbits. This suggests that the mean spectra are representative of average conditions in the magnetotail and no transient events (e.g., geomagnetic storms) have a disproportionate effect of the average PADs, which may have been the case if data for any β_p bin were taken from only a few orbits. Every β_p bin had at least 200 electron and 100 proton PADs, with the majority of bins containing over 1,000 distributions. These good counting statistics suggest that the mean values plotted in Figures 2 and 3 are well-defined. Spectrograms of the standard error on these means, expressed as a percentage of the mean flux and included in the auxiliary material for this letter, confirm this.[1] Where there are significant fluxes and more than 1,000 PADs per bin, the standard error on the mean is generally ~1%. For larger values of β_p the standard error does not increase past ~15% and is more often closer to ~4%. Note that the standard deviation is higher (≥40% where there significant fluxes), reflecting the natural variability of the magnetotail

[cf. *Baumjohann et al.*, 1989]. Reducing the bin size and hence increasing the samples in each bin did not significantly reduce the standard deviation.

4. Discussion and Conclusions

[17] The proton observations described in Figure 2 generally conform to the accepted picture of magnetotail ion populations. At the lowest values of β_p, protons at higher energies flow Earthward (Figure 2d) - perhaps a manifestation of the time-varying beamlets [*Ashour-Abdalla et al.*, 2005] that would be expected in averages such as those we present here. This is also consistent with the unidirectional beams historically observed at the outer edge of the PSBL [*Parks et al.*, 1984]. At lower energies tailward flowing protons dominate the field aligned components of the PAD, possibly representing ionospheric outflow. The transition from unidirectional, Earthward beams of protons to bidirectional beams at $\beta_p \sim 0.3$ is also consistent with the canonical evolution of the PSBL from the lobe towards the CPS [*Parks et al.*, 1984] and can be explained as the arrival of mirrored protons that coexist with the Earthward beams. The transition to more isotropic proton PADs, i.e., the CPS, at $\beta_p \sim 3$ is also consistent with the expected structure of the magnetotail. These results however, differ from those of *Baumjohann et al.* [1988, 1989] in that the transition from PSBL to CPS, when one defines the CPS as being dominated by isotropic protons, occurs when $\beta_p \sim 3$ - the boundary of the inner CPS as defined by *Baumjohann et al.* [1989]. This suggests that the use of $\beta_p > 0.5$ to identify the plasma sheet is perhaps an underestimate.

[18] The bidirectional electrons observed for $\beta_p < 0.05$ (Figures 3a and 3b) are presumably the polar rain population that enters the magnetosphere from the solar wind, flowing Earthward along open field lines [e.g., *Alexeev et al.*, 2006], some of which then mirror and combine with ionospheric outflow, resulting in a slightly higher net flux of tailward electrons in regions with low β_p (Figure 3d). The dominance of bidirectional electrons at low energies for all β_p (Figure 3e) presumably represents the electron population identified by *Åsnes et al.* [2008] and seems to have a counterpart in the protons, albeit one existing over a more restricted range of β_p (Figure 2e). Unlike the protons, and contrary to the canonical picture of the magnetotail, no extended isotropic electron CPS is evident in Figure 3. Bidirectional electrons dominate at all energies for $0.7 < \beta_p < 17$, the range that could be described as an electron PSBL (Figure 3e). For values of $\beta_p > 17$, however there is a small region of isotropy, quickly giving way to electrons with perpendicular-dominated PADs that exist at only the highest values of β_p, i.e., close to the neutral sheet.

[19] That the electrons and protons exhibit such different behavior, to the extent that there does not, on average, appear to be an isotropic electron plasma sheet, and that field-aligned electrons are scattered in pitch angle at much higher β_p then protons, suggests that the electrons and protons are acted on either by different physical processes, or that the same processes act differently on electrons and ions. One such process is the nonadiabatic acceleration of particles as they pass through the magnetotail current sheet [e.g., *Tsyganenko*, 1982] which has been shown to isotropize ions in only a few encounters with the current sheet [e.g., *Sergeev et al.*, 1983]. Electrons are less likely to behave nonadiabatically than protons because of their smaller gyroradii. Another possibility for preferential pitch angle scattering of protons is their interaction with ULF waves observed to be present in the PSBL during so-called "harmonic events" [*Engebretson et al.*, 2010]. Ion distributions measured during these events have been shown to be unstable to the observed wave modes, whereas the contemporaneous electron distributions were found to be stable [*Denton et al.*, 2010]. Neither of these processes, however, explain the rapid transition from bidirectional to perpendicular dominated electron PADs at the highest values of β_p, which remains the subject of further work. We note here that the observed Earthward proton fluxes at low beta (Figure 2a) are too low to account for the observed isotropic CPS fluxes, so pitch angle scattering of these particles cannot exclusively be responsible for the formation of the CPS. Other processes, such as diffusion from the flanks or the scattering of field-aligned particles tailward of Cluster, such that they are not measured in our study, must also play a part.

[20] In conclusion, the results of this first systematic survey of magnetotail PADs measured by Cluster suggest that the typical value of $\beta = 0.5$ used to identify the CPS is perhaps an underestimate: Isotropic protons are only routinely seen when $\beta_p > 3$. Furthermore there is no evidence for an extended, isotropic, electron plasma sheet. Instead a rapid transition from bidirectional to perpendicular electron PADs is observed at $\beta_p \sim 17$. We suggest that either non-adiabatic acceleration processes or wave-particle interactions may contribute to the isotropization of CPS protons, however the mechanism responsible for the pitch angle scattering of electrons is still unknown.

[22]   The Editor thanks O. Walter Lennartsson and an anonymous reviewer for their assistance in evaluating this paper.

References

Alexeev, I. V., V. Sergeev, C. J. Owen, A. Fazakerley, E. Lucek, and H. Rème (2006), Remote sensing of a magnetotail reconnection X-line using polar rain electrons, *Geophys. Res. Lett.*, *33*, L19105, doi:10.1029/2006GL027243.

Angelopoulos, V., W. Baumjohann, C. F. Kennel, F. V. Coroniti, M. G. Kivelson, R. Pellat, R. J. Walker, H. Lühr, and G. Paschmann (1992), Bursty bulk flows in the inner central plasma sheet, *J. Geophys. Res.*, *97*, 4027–4039.

Ashour-Abdalla, M., J. M. Bosqued, M. El-Alaoui, V. Peroomian, L. M. Zelenyi, R. J. Walker, and J. Wright (2005), A stochastic sea: The source of plasma sheet boundary layer ion structures observed by Cluster, *J. Geophys. Res.*, *110*, A12221, doi:10.1029/2005JA011183.

Åsnes, A., M. G. Taylor, and C. Simon (2008), Aurora secondary electrons in the plasma sheet: A Cluster study, *Eos Trans. AGU*, *89*(53), Fall Meet. Suppl., Abstract SM24A-07.

Balogh, A., et al. (2001), The Cluster magnetic field investigation: Overview of in-flight performance and initial results, *Ann. Geophys.*, *19*, 1207–1217.

Baumjohann, W., G. Paschmann, N. Sckopke, C. A. Cattell, and C. W. Carlson (1988), Average ion moments in the plasma sheet boundary layer, *J. Geophys. Res.*, *93*, 11,507–11,520, doi:10.1029/JA093iA10p11507.

Baumjohann, W., G. Paschmann, and C. A. Cattell (1989), Average plasma properties in the central plasma sheet, *J. Geophys. Res.*, *94*, 6597–6606, doi:10.1029/JA094iA06p06597.

Cully, C. M., R. E. Ergun, and A. I. Eriksson (2007), Electrostatic structure around spacecraft in tenuous plasmas, *J. Geophys. Res.*, *112*, A09211, doi:10.1029/2007JA012269.

Denton, R. E., M. J. Engebretson, A. Keiling, A. P. Walsh, S. P. Gary, P. M. E. Décréau, C. A. Cattell, and H. Rème (2010), Multiple harmonic ULF waves in the plasma sheet boundary layer: Instability analysis, *J. Geophys. Res.*, *115*, A12224, doi:10.1029/2010JA015928.

Engebretson, M. J., C. R. G. Kahlstorf, J. L. Posch, A. Keiling, A. P. Walsh, R. E. Denton, M. C. Broughton, C. J. Owen, K.-H. Fornaçon, and H. Rème (2010), Multiple harmonic ULF waves in the plasma sheet boundary layer observed by Cluster, *J. Geophys. Res.*, *115*, A12225, doi:10.1029/2010JA015929.

Gustafsson, G., et al. (2001), First results of electric field and density observations by Cluster EFW based on initial months of operation, *Ann. Geophys.*, *19*, 1219–1240.

Johnstone, A. D., et al. (1997), PEACE: A plasma electron and current experiment, *Space Sci.Rev.*, *79*, 351–398.

Onsager, T. G., M. F. Thomsen, R. C. Elphic, and J. T. Gosling (1991), Model of electron and ion distributions in the plasma sheet boundary layer, *J. Geophys. Res.*, *96*, 20,999–21,011, doi:10.1029/91JA01983.

Parks, G. K., et al. (1984), Particle and field characteristics of the high-latitude plasma sheet boundary layer, *J. Geophys. Res.*, *89*, 8885–8906, doi:10.1029/JA089iA10p08885.

Parks, G. K., L. J. Chen, M. Fillingim, and M. McCarthy (2001), Kinetic characterization of plasma sheet dynamics, *Space Sci. Rev.*, *95*, 237–255.

Rème, H., et al. (2001), First multispacecraft ion measurements in and near the Earth's magnetosphere with the identical Cluster ion spectrometry (CIS) experiment, *Ann. Geophys.*, *19*, 1303–1354.

Sergeev, V. A., E. M. Sazhina, N. A. Tsyganenko, J. A. Lundblad, and F. Soraas (1983), Pitch-angle scattering of energetic protons in the magnetotail current sheet as the dominant source of their isotropic precipitation into the nightside ionosphere, *Planet. Space Sci.*, *31*, 1147–1155.

Smets, R., D. Delcourt, J. A. Sauvaud, and P. Koperski (1999), Electron pitch angle distributions following the dipolarization phase of a substorm: Interball-Tail observations and modeling, *J. Geophys. Res.*, *104*, 14,571–14,581, doi:10.1029/1998JA900162.

Tsyganenko, N. A. (1982), Pitch-angle scattering of energetic particles in the current sheet of the magnetospheric tail and stationary distribution functions, *Planet. Space Sci.*, *30*, 433–437.

Zhang, T. L., et al. (2006), A statistical survey of the magnetotail current sheet, *Adv. Space Res.*, *38*, 1834–1837, doi:10.1016/j.asr.2006.05.009.

I. Dandouras, Centre d'Etude Spatiale des Rayonnements, Université de Toulouse, BP 44346, 9 Av. du Colonel Roche, F-31028 Toulouse CEDEX, France.

A. N. Fazakerley, C. Forsyth, C. J. Owen, and A. P. Walsh, Mullard Space Science Laboratory, University College London, Holmbury St. Mary, Dorking RH5 6NT, UK. (apw@mssl.ucl.ac.uk)